HHS Public Access

Author manuscript

J Magn Reson. Author manuscript; available in PMC 2018 March 01.

Published in final edited form as:

J Magn Reson. 2017 March ; 276: 78–85. doi:10.1016/j.jmr.2017.01.014.

NMR Spin-Lock Induced Crossing (SLIC) Dispersion and Long-Lived Spin States of Gaseous Propane at Low Magnetic Field (0.05 T)

Danila A. Barskiy[*,a,b], **Oleg G. Salnikov**[c,d], **Alexey S. Romanov**[c,d], **Matthew A. Feldman**[a,b], **Aaron M. Coffey**[a,b], **Kirill V. Kovtunov**[c,d], **Igor V. Koptyug**[c,d], and **Eduard Y. Chekmenev**[*,a,b,e,f,g]

[a]Institute of Imaging Sciences, Vanderbilt University, Nashville, TN 37232, USA

[b]Department of Radiology, Vanderbilt University, Nashville, TN 37232, USA

[c]International Tomography Center, 3A Institutskaya st., Novosibirsk, Russia

[d]Novosibirsk State University, 2 Pirogova st., Novosibirsk, Russia

[e]Department of Biomedical Engineering, Vanderbilt University, Nashville, TN 37232, USA

[f]Vanderbilt Ingram Cancer Center, Vanderbilt University, Nashville, TN 37232, USA

[g]Russian Academy of Sciences, Moscow, Russia

Abstract

When parahydrogen reacts with propylene in low magnetic fields (*e.g.*, 0.05 T), the reaction product propane develops an overpopulation of pseudo-singlet nuclear spin states. We studied how the spin-lock induced crossing (SLIC) technique can be used to convert these pseudo-singlet spin states of hyperpolarized gaseous propane into observable magnetization and to detect ^{1}H NMR signal directly at 0.05 T. The theoretical simulation and experimental study of the NMR signal dependence on B_1 power (SLIC amplitude) exhibits a well-resolved dispersion, which is induced by the spin-spin couplings in the eight-proton spin system of propane. We also measured the exponential decay time constants (T_{LLSS} or T_S) of these pseudo-singlet long-lived spin states (LLSS) by varying the time between hyperpolarized propane production and SLIC detection. We have found that, on average, T_S is approximately 3 times longer than the corresponding T_1 value under the same conditions in the range of pressures studied (up to 7.6 atm). Moreover, T_S may exceed 13 seconds at pressures above 7 atm in the gas phase. These results are in agreement with the previous reports, and they corroborate a great potential of long-lived hyperpolarized propane as an inhalable gaseous contrast agent for lung imaging and as a molecular tracer to study porous media using low-field NMR and MRI.

[*]Corresponding authors: danila.barskiy@vanderbilt.edu (Danila A. Barskiy) eduard.chekmenev@vanderbilt.edu (Eduard Y. Chekmenev).

Supporting Information: Additional supporting information may be found in the online version of this article at the publisher's web site.

Keywords

NMR; MRI; low field; hyperpolarization; parahydrogen; long-lived spin states; propane

1. Introduction

Low-field hyperpolarized (HP) nuclear magnetic resonance (NMR) spectroscopy and imaging (MRI) are quickly developing frontiers of magnetic resonance research.[1] The recent boost of interest in low-field NMR/MRI can be explained by three primary reasons. First, several hyperpolarization techniques rapidly emerged, which enhance NMR signals by orders of magnitude,[2] thereby significantly improving the signal-to-noise ratio (SNR). Second, improvements in detection sensitivity of low-field NMR/MRI (*e. g.*, High-Quality-factor-Enhanced NMR or EHQE-NMR[3]) enable approaching or even exceeding the sensitivity of conventional high-field NMR/MRI.[4] Third, the lifetime of the hyperpolarized state can be significantly enhanced at low magnetic fields for protons and/or heteronuclei either through reduced contribution from chemical shift anisotropy or through long-lived spin states (LLSS).[5-13] These advantages make low-field hyperpolarized NMR/MRI a promising modality for *in vivo* molecular spectroscopy and imaging.[14-18] Moreover, MRI in fields below 0.1 T offers the additional advantage of negligible Specific Absorption Rate (SAR), therefore providing enhanced patient safety and removing limitations on pulse sequence design and implementation.[19] While any hyperpolarization technique can be used in the context of low-field NMR/MRI, less expensive and more high-throughput parahydrogen-based hyperpolarization techniques, such as parahydrogen-induced polarization (PHIP)[20-22] and signal amplification by reversible exchange (SABRE),[23-28] are naturally more suited to go hand-in-hand with an inexpensive low-field MR modality rather than the more expensive (millions of dollars) and low-throughput technique of dissolution dynamic nuclear polarization (d-DNP),[29-30] currently the leading hyperpolarization technology.[1, 31-32] It is also worth emphasizing that the maximum polarization obtainable by d-DNP depends strongly on the applied magnetic field and spin temperature (since it is a phenomenon of polarization transfer from electrons to nuclei), whereas for PHIP and SABRE the maximum polarization is independent of these parameters. Furthermore, in addition to biomedical applications, the combination of hyperpolarization and low-field detection can be also potentially useful for spectroscopic and imaging analysis of industrial-scale processes, where overpopulated pseudo-singlet spin states are conveniently created using chemical reactions involving parahydrogen.[33]

Parahydrogen (p-H_2) is a naturally occurring nuclear spin singlet state that can be efficiently incorporated into certain molecules of interest via pairwise hydrogenation reaction.[20-21, 34] When the reaction is carried out in a sufficiently low magnetic field, the singlet spin state of the nascent p-H_2 protons can be relatively long-lived if permitted by the symmetry of the nuclear spin Hamiltonian.[35] The p-H_2-induced singlet spin order can be converted into observable magnetization using various singlet-to-magnetization (S2M) transfer algorithms,[36] including spin-lock induced crossing,[37-39] and conveniently detected directly at low field.[33]

Recently, we demonstrated that when parahydrogen is added to the molecule propylene at a relatively low magnetic field (*i.e.*, in the strong-coupling regime, where chemical shift difference between methylene and methyl protons of ~0.44 ppm in propane are less than their spin-spin coupling constant $^3J_{HH}$ of ~7.4 Hz), the symmetry of the *p*-H_2-nascent singlet state is partially conserved in the resultant propane molecule and that propane produced in this fashion may potentially possess LLSS.[40] This is not straightforward, because, firstly, propane is a multi-spin system containing 8 strongly coupled protons at low magnetic field, which is a significantly more complex spin system than the isolated 2-spin pairs typically exploited as LLSS.[41] Secondly, the dominant relaxation mechanism for molecules in the gas phase is often the modulation of spin-rotation interactions rather than dipole-dipole interactions, because dipole-dipole interactions are effectively "switched off" between spins in a singlet state.[42-43] Nevertheless, it has been shown theoretically[44-45] and experimentally[45-47] that LLSS can exist in multi-spin systems comprising more than two coupled spins.

Here, we present a systematic study of LLSS in the hyperpolarized gaseous propane molecule via (i) employing PHIP to produce gaseous propane at a low magnetic field and (ii) subsequently transforming the "hidden" pseudo-singlet spin order into observable magnetization using the Spin-Lock Induced Crossing (SLIC) technique[37, 48] and performing signal detection directly at 0.05 T (Figure 1a). Using a variable time delay (*i.e.*, wait time) between hyperpolarized propane production and signal detection, we were able to measure the lifetime (T_S) of the pseudo-singlet LLSS for a wide range of pressures, and T_S was found to be approximately 3-fold greater than T_1 under the same conditions. The very high SLIC transformation efficiency, which is enabled by the use of a more homogeneous magnet than in our pioneering report,[40] allowed us to demonstrate high-resolution ^{1}H NMR spectra and well-resolved dependence of the observable NMR signal on B_1 power (SLIC dispersion), which is clearly modulated by proton-proton *J*-couplings in the propane molecule. Finally, we performed spin dynamics simulations by solving the full Liouville–von Neumann equation, and demonstrated that the experimentally observed phenomena are in excellent agreement with theoretical calculations.

2. Materials and Methods

2.1. Heterogeneous hydrogenation

The schematic of the experimental setup is shown in Figure 1b. Propylene (>99%, Sigma-Aldrich, #295663) and ultra-pure hydrogen (>99.999%, A-L Compressed Gases Inc., Nashville, TN) were used as received. Preparation of the Rh/TiO_2 catalyst was described elsewhere.[49] Hydrogen gas was enriched with *p*-H_2 to ~50% *para*-state using a home-built parahydrogen generator by passing normal H_2 through FeO(OH) powder (Sigma-Aldrich, P/N 371254, 30–50 mesh) maintained at liquid N_2 temperature (77 K).[50] Alternatively, a home-built *p*-H_2 generator using cryocooling was employed to produce 80% *p*-H_2. Gas flow rates of *p*-H_2 and propylene (see SI for details regarding flow rates for different pressures) were regulated by mass flow controllers (Sierra Instruments, Monterey, CA, model #C50L-AL-DD-2-PV2-V0). The gases flowed through a long Teflon tube to ensure their efficient mixing and then to the 1/8 in. tubing copper reactor packed with Rh/TiO_2 catalyst located

between two pieces of packed fiberglass wool. The reactor was heated to 100 °C using heating tape. The resultant gas mixture was directed either to the detection chamber (a plastic chamber or medium walled 5 mm NMR tube) located inside the RF probe connected to the NMR spectrometer (Kea2, Magritek, Wellington, New Zealand) or directly to the vent using a system of two manual shut-off valves (Western Analytical Products, #P-733). The total pressure in the reactor and in the detection chamber was the same, and it was controlled using a backpressure regulator (Figure 1b).

2.2. Low-Field (2 MHz) NMR Detection

Two experimental arrangements were used to obtain data in the current study. The first experimental setup was similar to that described earlier.[33] The magnet (~2 MHz Magritek rock core analyzer, Halbach array, radial field direction) had homogeneity of ~20 ppm over 4 cm diameter of spherical volume (DSV). A commercially available MR Kea2 spectrometer (Magritek, Wellington, New Zealand) was used for NMR detection as described by Waddell et al.[51] The detection chamber (plastic, ~2 mL) was placed in the home-built ^{1}H RF coil located in the magnet.[52] More experimental details of this experimental arrangement can be found in Ref. [33].

The second arrangement of the low-field NMR apparatus was comprised of a shimmed permanent magnet (SIGWA 0.0475T, Boston, MA) with an 80 cm gap and a homogeneity of <20 ppm across a 40 cm DSV (note that B_0 homogeneity over the relevant volume of the 5 mm NMR tube was better than 2 ppm) and a two channel RF probe consisting of an inner Tx/Rx detection coil and an outer Tx-only excitation coil. The two channel ^{1}H/^{1}H RF probe was designed to measure samples stored in standard 5 mm diameter NMR tubes (see SI). The inner Tx/Rx solenoid RF coil was decoupled from the outer transmit-only Helmholtz saddle coil by geometric orthogonality. The solenoid coil constructed conformed closely to the dimensions of the NMR sample (8 mm diameter by 193 mm length) in order to improve the coil filling factor and had a quality factor Q of 70. This experimental arrangement allowed attenuating the SLIC RF pulses from the output of the RF amplifier (BT00250-AlphaS, Tomco, Stepney, South Australia) without attenuating the detected NMR signal coming from the spin system after pulses. The coil was shielded from electric field interference and noise by housing it in a RF shield composed of a hollow copper cube made out of square copper clad PCB material (1 ft × 1 ft). A circular waveguide 50 mm in length protruded from the shield and served as an access port for insertion of the sample into the RF coil. The shielding provided an electric field suppression of 60 dB. Radio frequency calibration of the Tx/Rx coil using a 10 mM aqueous solution of $CuSO_4$ in a 5 mm medium walled NMR tube yielded a $\pi/2$ ^{1}H excitation pulse width of 26 μs at 0.6 W. Most of the experimental results presented in the study were obtained using the second arrangement (unless otherwise noted).

2.3. SLIC RF Pulse Sequence

Spin order of *p*-H_2-nascent protons after chemical addition to propylene was converted to observable magnetization using the Spin-Lock Induced Crossing (SLIC) sequence developed by DeVience et al.[37] In order to generate low-power (~30 μW) SLIC pulses, additional attenuators (Bird Technologies, 10 W, A series, male/female N connector, 30 and 20 dB)

were inserted between the output of the second RF amplifier and the RF input of the Tx coil. The SLIC pulse amplitude was calibrated by measuring the signal of a 10 mM aqueous solution of $CuSO_4$ (placed in a 5 mm medium walled NMR tube) on the Tx/Rx coil while transmitting on the Tx-only channel. Nutation experiments for the Tx-only coil at the power level of SLIC pulses (32 μW) with detection via the Tx/Rx coil yielded $\pi/2$ ^{1}H excitation pulse width of 22 ms. Acquisition of the ^{1}H NMR signal occurred directly during the flow of the propane gas through the NMR tube. The lifetime (T_S) of the pseudo-singlet LLSS of propane in 0.05 T field was measured by varying the time delay between the interruption of gas flow through the detection chamber and the application of the SLIC pulse. For T_1 measurements, the pulse sequence was applied immediately after the gas flow was stopped.

3. Results and Discussion

The intensity of an NMR signal is directly proportional to the product of the nuclear spin polarization and the concentration of magnetic nuclei in the detection zone of the NMR spectrometer. Both of these parameters are very low for thermally polarized propane at a magnetic field of 0.05 T. Indeed, at such a low field the thermal polarization of ^{1}H nuclei is only $1.6 \cdot 10^{-5}$% and the concentration of hydrogen atoms in gaseous propane is ~0.3 M, which is approximately two orders of magnitude lower than the proton concentration in liquid water. The PHIP hyperpolarization technique is suitable for direct ^{1}H NMR signal enhancement of the propane, when the chemical shift difference between *p*-H_2-nascent protons is significantly greater than the $^3J_{HH}$-coupling between them. This corresponds to the condition of the weak coupling regime for methyl and methylene protons in the propane molecule. Otherwise, in the strong coupling regime, the singlet state of *p*-H_2 is still conserved in the propane molecule produced by hydrogenation of propylene. This manifests itself in a relatively low NMR signal when measured at low magnetic field, because the PHIP-induced quantum state is nonmagnetic. Indeed, a direct detection of hyperpolarized (HP) propane using a $\pi/2$ hard pulse at 0.05 T results in a relatively low-intensity antiphase signal, showing a complex splitting pattern (Figure 2a). This result is in accordance with the previously reported low-field NMR detection of HP norbornane.[53] We also note that this complex spectral pattern was not fully spectrally resolved earlier due to significantly worse B_0 magnetic field homogeneity.[40] We carried out spin dynamics simulations by numerically solving the Liouville–von Neumann equation for the density matrix of the spin system in order to analyze this pattern and to rationalize the observed splittings (see SI). The analysis revealed that the dominant contribution to the observed ^{1}H NMR signal is from the propane molecules containing ^{13}C nuclei at natural abundance (1.1%). The calculation included only a one-bond heteronuclear *J*-coupling of 125 Hz and three equally probable positions of the ^{13}C label with respect to the *p*-H_2-nascent protons in the propane molecule (Figure 2b). The simulated spectrum reproduces very well the observed experimental features (Figure 2b), and the resulting NMR spectrum is essentially dominated by the signal originating from ^{13}C-containing isotopomers. This is remarkable, because ^{13}C-containing isotopomers account for only ~3.3% of all propane molecules, while the bulk of the propane (~96.7%) is free from magnetic nuclei other than protons. Nevertheless, this small population of ^{13}C-containing isotopomers produces the vast fraction of the observed NMR signal.

A much greater NMR signal intensity from ^{13}C-containing HP propane molecules (compared to those without ^{13}C nuclei) is the presence of *J*-coupled heteronucleus (*i.e.* ^{13}C). This heteronucleus (*i.e.* ^{13}C) breaks the near magnetic equivalence of strongly coupled hydrogen nuclei due to unequal heteronuclear couplings to different protons in the molecule and reveals the otherwise "hidden" *p*-H_2-induced hyperpolarization. This observation is similar to propane-d_6 produced via *p*-H_2 pairwise addition to propylene-d_6 demonstrating significantly stronger NMR signals than its non-deuterated analogue using direct detection and hard excitation RF pulses at 0.05 T.[54] Note that if a $\pi/4$ pulse is used for signal detection, the observed ^{1}H NMR spectrum is slightly different (however, it can be very well simulated using a density matrix formalism), mainly because of the significantly altered spectral contribution of ^{13}C-containing isotopomers (Figure S5).

When a SLIC RF pulse is used for excitation, it yields an NMR signal 1-2 orders of magnitude greater than that obtained using a hard RF pulse excitation (Figure 2c). The SLIC RF pulse employed had a duration (τ_{slic}) of ~0.5 s and a B_1 amplitude of ~22.2 Hz. The latter corresponds to approximately $3 \cdot {}^3J_{HH}$, where $^3J_{HH}$ is the three-bond spin-spin coupling constant between methyl and methylene protons in propane. Spectral simulations support our experimental finding, *i.e.,* the observation of the in-phase NMR signal of HP propane after SLIC RF excitation (Figure 2d). The dominant fraction of this signal is the contribution from the most abundant HP propane molecules without ^{13}C nuclei. The experimentally observed NMR signal intensity was approximately 14 times lower than that predicted theoretically (if the corresponding spectra obtained with a $\pi/2$ pulse are normalized to have the same signal intensity, see Figure 2a-d). This discrepancy cannot be explained by relaxation losses before acquisition; indeed, the time HP propane spent between production and the detection was the same in both detection protocols in which the hard pulse and the SLIC pulse were utilized (Figures 2a and 2c). More than a factor of 14 difference in signal intensities may be partially explained by a non-ideal performance of the SLIC pulse, caused by inhomogeneity of B_1 and B_0 fields (most critical factor) and relaxation/decoherence during the long RF SLIC excitation pulse (0.5 s).[33] More importantly, these experiments were performed in a continuous flow mode, where gaseous propane was flowing through the NMR tube while the NMR signal was being acquired. As a result, a significant fraction of the produced HP propane might have migrated into or out of the RF coil during the SLIC pulse. This fact can additionally significantly lower the resulting SLIC-induced signal. However, performing the experiment in the continuous flow regime is a clear advantage of the present study, because the critical parameters influencing the SLIC efficiency (*i.e.,* τ_{slic} and B_1) can be conveniently studied in an automated fashion under nearly identical conditions.

Next, the B_1 amplitude of the SLIC pulse was varied under conditions of fixed τ_{slic} of ~0.5 s. The resulting NMR signal peak intensity was plotted as a function of B_1 amplitude revealing a notable quartet splitting pattern (Figure 2e). We deem this spectral pattern 'SLIC dispersion' (in a manner similar to chemical shift dispersion), which is clearly mediated by the three-bond H-H spin-spin coupling $^3J_{HH}$ due to the peaks' positions at ~7.4 Hz, ~14.8 Hz, ~22.2 Hz, and ~29.6 Hz, respectively. It should also be emphasized that the asymmetry of this quartet (*i.e.,* lower peak intensity at lower B_1 values) is likely the result of disproportionately greater signal losses due to B_1 and B_0 inhomogeneities. The observed

pattern is also significantly more complex than the analogous one for a two-spin system, where (i) there are no additional spin-spin couplings, and (ii) a maximum is observed for B_1 value equal to the value of spin-spin coupling J.[37] Spin dynamics calculations using the density matrix formalism were carried out in order to explain the experimental results (see SI). We found that if the frequency (B_1 offset) of the SLIC pulse is set exactly at the average of the methyl and methylene proton resonances and τ_{slic} = 0.5 s, the maxima in signal amplitude are observed at the frequencies $^3J_{HH}$, $2\cdot{}^3J_{HH}$, $3\cdot{}^3J_{HH}$, and $4\cdot{}^3J_{HH}$, where $^3J_{HH}$ is the spin-spin coupling constant between methyl and methylene protons (Figure 2e). This result is reasonable, because nuclear spin level anti-crossings (spin-lock induced crossings) occur at specific nutation frequencies. At these frequencies, chemical shift differences drive a polarization transfer between spin-locked states with $\Delta F = \pm 1$ and $\Delta m_F = \pm 1$, where F and m_F are angular momentum quantum numbers (*i.e.*, states$|F, m_F\rangle$, which is detected as a decrease in x-axis magnetization (*i.e.*, observable signal).[55]

The dependence of the ^{1}H NMR signal of HP propane on the duration of the SLIC pulse is shown in Figure 2f. It manifests itself as a decaying oscillation reaching a plateau at approximately half of the maximal intensity for τ_{slic} greater than 2 s. The main reason for this plateauing (vs. signal decaying to zero) is the experimental condition of continuous gas flow through the NMR tube during the series of acquisitions with variable SLIC duration. Whilst a portion of the gas was most likely pushed out by the inflowing gas, the freshly supplied HP propane portion experiences only a fraction of the SLIC pulse. After a certain duration of the SLIC pulse the observed signal becomes independent of τ_{slic} and a steady-state magnetization is achieved. An analytical solution for the SLIC signal vs. SLIC duration in the present experimental arrangement is in agreement with the observed phenomena and is presented in the SI (Figure S8).

The T_S and T_1 of HP propane were measured at 0.05 T using optimal values of B_1 amplitude and τ_{slic} found for the SLIC RF pulse, Figures 3a,b. Specifically, the pulse sequences shown in Figures 3c-f were employed. The waiting time period between the injection of the gas into the detection chamber and the application of the SLIC pulse was varied in a consecutive series of experiments for T_S measurements. Since the SLIC RF pulse allows converting the singlet spin state directly into transverse magnetization, no additional RF pulses are needed for measuring T_S (Figures 3c,d). In case of T_1 measurements, the SLIC RF pulse was applied directly after the injection of HP propane gas into the chamber, immediately followed by a $\pi/2$ pulse to convert transverse magnetization created by the SLIC pulse into a longitudinal one (parallel to the z-axis). Then two different strategies were used for the measurement. In the first approach, small-angle RF excitation pulses were employed to probe the T_1. The second strategy used a variable delay between rotating the magnetization toward the z-axis and applying the second $\pi/2$ pulse. Measured values are plotted in Figure 3b, and in addition listed in Table S1. Two representative curves are shown in Figure 3a for the pressure of ~7.6 atm.

Both T_1 and T_S of HP propane increase with the total gas pressure (up to T_1 ~4 s and T_S ~13 s at 7.6 atm). This is not surprising, because the correlation time is reduced when the collision time between gas molecules decreases. Another potential reason for T_1 and T_S becoming longer is the greater fraction of HP propane in the gas phase as pressure increases

due to changes in propylene hydrogenation kinetics.[56-57] Indeed, additional ^{1}H 400 MHz NMR measurements using the same experimental setup demonstrated that propylene to propane conversion increases as the total pressure increases (see SI). This fact is in agreement with typically positive overall reaction orders for hydrogenation of alkenes above 300 K.[56, 58-62] Notably, the experimentally determined ratio of T_S/T_1 is nearly constant and amounts to 3.1±0.5 for all studied pressures, suggesting that the contribution of dipole-dipole interaction modulation towards the relaxation mechanism for hydrocarbons in general, and propane in particular, is significant. Future studies are certainly warranted to investigate theoretically the fundamental causes governing the observed behavior and multi-spin proton LLSS in the gas phase.

Analysis of static magnetic fields suitable for the SLIC transformation in propane was carried out. In general, the static magnetic field (B_0) should be low enough for p-H_2-nascent protons to reside in singlet spin states after hydrogenation. Straightforward analysis shows that for two p-H_2-nascent spins in methylene and methyl groups to be in the strong coupling regime, a magnetic field B_0 below $2\pi J/\gamma_{1H}(\delta_1 - \delta_2)$ T is sufficient (here γ_{1H} is the proton gyromagnetic ratio, J = 7.4 Hz is the spin-spin coupling between methylene and methyl protons, and δ_1 = 1.34 ppm and δ_2 = 0.9 ppm are their chemical shifts, respectively). Our simulations show that the optimal duration of the SLIC pulse may be decreased from ~600 ms at 0.05 T down to ~70 ms at 0.4 T (see SI). This will undoubtedly improve the overall performance of the SLIC pulse in singlet-to-triplet conversion, because relaxation/decoherence losses during the spin-lock pulse will be reduced. Moreover, the ^{1}H NMR signal of propane obtained after the SLIC pulse may be increased at higher fields as well (Figure S6). Moving to magnetic fields higher than 0.05 T as employed here has other advantages: MRI scanners operating in the low magnetic field region (*i.e.*, 0.1-0.5 T) are readily available on the market. Given that relaxation times (T_1, T_2, and T_S) of propane should not significantly depend on the static magnetic field strength (since the conditions of extreme narrowing apply for propane in the gas phase[58]), operation in the 0.1-0.5 T magnetic field region may additionally improve SLIC efficiency and signal detection sensitivity of HP gaseous propane for various applications.

The singlet-to-triple conversion efficiency can approach a theoretical limit of unity or 100% only in case of ideal (*i.e.* two isolated proton spin system, Figure S7b), while the transformation efficiency at 0.05 T was found ~8% for a propane eight-proton spin system in our experiments. While this value is significantly is significantly below 100%, it is the manifestation of a complex network of spin-spin interaction. Indeed, system simplification to five (versus eight) proton spins of ethyl group results in the increase of transformation efficiency to ca. 14% using otherwise the same simulation parameters. This observation is also in agreement with our previous SLIC studies ethyl groups in the liquid state. It should be pointed out that SLIC transformation efficiency of propane can be more than doubled (and exceed 18%) at higher magnetic fields, *e.g.* using 0.4 T versus 0.05 T, Figures S6.

The results presented here are important in the context of potential applications of HP propane and its LLSS created by pairwise addition of p-H_2 as an inhalable contrast agent for functional lung imaging. Several clinical research approaches for lung imaging using MRI that are currently being developed include imaging of heteronuclei, *e.g.* ^{19}F MRI of

perfluorinated gases such as SF_6 and C_nF_{2n+2} (n=1-3)[63-64] or HP noble gases, such as ^{3}He, ^{129}Xe, and others.[31, 65-66] The production of HP noble gases is relatively high cost, and it also requires sophisticated hyperpolarizer instrumentation. The imaging of both HP noble gases and ^{19}F via MRI additionally requires multinuclear RF coil and transmitter/receiver capabilities. The above two factors significantly limit applications of these agents only to several privileged centers of excellence worldwide. The major advantage of using HP propane (and potentially other hydrocarbon gases)[67] in MRI is its very low cost (a few cents per liter excluding the cost of p-H_2 production) and production scalability. Moreover, any MRI system with proton transmit/receive circuitry is potentially capable of molecular imaging using HP propane; it should be noted though that LLSS may be currently utilized using low-field MRI scanners.[33] Furthermore, ^{1}H MRI of hydrocarbon gases may find various applications in materials science, studying porous media, imaging of chemical reactors, or other non-biomedical applications.

It is important to consider the key contrast agent characteristics influencing the detection sensitivity of HP propane compared to that of HP ^{129}Xe in the context of potential biomedical applications. Hyperpolarization of ^{129}Xe to nearly the theoretical maximum of unity (~90%) has been demonstrated,[68-70] while the highest propane polarization demonstrated to date is only 6%.[71] However, more than 3 times greater gyromagnetic ratio of protons compared to that of ^{129}Xe and the widespread availability of ^{1}H transmitter/detection hardware in MRI scanners make them much more favorable nuclei from the detection perspective for hyperpolarized gas NMR/MRI. We hope that this study will stimulate future work to further increase the level of hyperpolarization of propane via PHIP. Finally, SLIC efficiency of singlet-to-triplet transformation is another challenge that should be addressed in the future to maximize the imaging capability of HP propane produced by PHIP.

4. Conclusion

In conclusion, the long-lived nuclear spin states of HP propane produced via pairwise addition of p-H_2 to propylene were systematically studied in the gas phase at pressures up to ~7.6 atm. In particular, we created the LLSS in HP propane gas and measured its exponential decay constant (T_S) by using hydrogenation of propylene with p-H_2 and subsequent NMR detection at 0.05 T employing a SLIC RF pulse. The T_1 and T_S measurements were carried out in sufficiently low magnetic field (*i.e.*, 0.05 T), where methyl and methylene protons of HP propane molecules are strongly coupled via three-bond spin-spin coupling $^3J_{HH}$. SLIC allows converting typically non-observable nuclear spin order of p-H_2-derived pseudo-singlet state of HP propane into readily observable transverse magnetization, and enables detecting ^{1}H NMR signal directly at low magnetic field. The lifetime of pseudo-singlet nuclear spin states of PHIP-produced HP propane is approximately 3 times greater than the corresponding T_1 time under the same reaction conditions. Moreover, a T_S value of at least 13 seconds in the gas phase is reported. These results of a relatively long decay constant and the demonstration of SLIC conversion highlight the great potential of HP propane produced by PHIP technique as an inhalable gaseous contrast agent for MRI of lungs (in the context of molecular imaging immediately

after inhalation of HP propane gas by a patient) and for other imaging application with the use of low-field MR instruments.

Supplementary Material

Refer to Web version on PubMed Central for supplementary material.

Acknowledgments

We gratefully acknowledge the financial support by NIH 1R21EB018014, 1R21EB020323, and 1F32EB021840, NSF CHE-1416268 and CHE-1416432, DOD CDMRP W81XWH-12-1-0159/BC112431, W81XWH-15-1-0271 and W81XWH-15-1-0272. The Russian team thanks the Russian Foundation for Basic Research (RFBR, grant 16-03-00407) for financial support.

References

1. Blümich B. Virtual special issue: Magnetic resonance at low fields. J Magn Reson. 2016; doi: 10.1016/j.jmr.2016.10.005
2. Nikolaou P, Goodson B, Chekmenev E. NMR Hyperpolarization Techniques for Biomedicine. Chem Eur J. 2015; 21:3156–3166. [PubMed: 25470566]
3. Suefke M, Liebisch A, Blumich B, Appelt S. External High-quality-factor Resonator Tunes Up Nuclear Magnetic Resonance. Nat Phys. 2015; 11:767–771.
4. Coffey A, Truong M, Chekmenev E. Low-field MRI Can Be More Sensitive Than High-field MRI. J Magn Reson. 2013; 237:169–174. [PubMed: 24239701]
5. Levitt M. Singlet Nuclear Magnetic Resonance. Annu Rev Phys Chem. 2012; 63:89–105. [PubMed: 22224703]
6. Carravetta M, Johannessen OG, Levitt MH. Beyond the T_1 limit: singlet nuclear spin states in low magnetic fields. Phys Rev Lett. 2004; 92:153003. [PubMed: 15169282]
7. Carravetta M, Levitt MH. Theory of long-lived nuclear spin states in solution nuclear magnetic resonance. I. Singlet states in low magnetic field. J Chem Phys. 2005; 122:214505. [PubMed: 15974752]
8. Pileio G, Carravetta M, Hughes E, Levitt MH. The long-lived nuclear singlet state of ^{15}N-nitrous oxide in solution. J Am Chem Soc. 2008; 130:12582–3. [PubMed: 18729363]
9. Pileio G, Carravetta M, Levitt MH. Storage of nuclear magnetization as long-lived singlet order in low magnetic field. Proc Natl Acad Sci USA. 2010; 107:17135–9. [PubMed: 20855584]
10. Theis T, Ortiz GX, Logan AW, Claytor KE, Feng Y, Huhn WP, Blum V, Malcolmson SJ, Chekmenev EY, Wang Q. Direct and cost-efficient hyperpolarization of long-lived nuclear spin states on universal $^{15}N_2$-diazirine molecular tags. Sci Adv. 2016; 2:e1501438. [PubMed: 27051867]
11. Vasos P, Comment A, Sarkar R, Ahuja P, Jannin S, Ansermet JP, Konter J, Hautle P, Van den Brandt B, Bodenhausen G. Long-lived states to sustain hyperpolarized magnetization. Proc Natl Acad Sci USA. 2009; 106:18469–18473. [PubMed: 19841270]
12. Warren W, Jenista E, Branca R, Chen X. Increasing Hyperpolarized Spin Lifetimes Through True Singlet Eigenstates. Science. 2009; 323:1711–1714. [PubMed: 19325112]
13. Roy SS, Norcott P, Raynern PJ, Green GGR, Duckett SBA. Hyperpolarizable 1H Magnetic Resonance Probe for Signal Detection 15 Minutes after Spin Polarization Storage. Angew Chem Int Ed. 2016; doi: 10.1002/anie.201609186
14. Patz S, Muradian I, Hrovat MI, Ruset IC, Topulos G, Covrig SD, Frederick E, Hatabu H, Hersman F, Butler JP. Human pulmonary imaging and spectroscopy with hyperpolarized ^{129}Xe at 0.2 T. Acad Radiol. 2008; 15:713–727. [PubMed: 18486008]
15. Parra-Robles J, Cross AR, Santyr GE. Theoretical signal-to-noise ratio and spatial resolution dependence on the magnetic field strength for hyperpolarized noble gas magnetic resonance imaging of human lungs. Med Phys. 2005; 32:221–229. [PubMed: 15719973]

16. Dominguez-Viqueira W, Parra-Robles J, Fox M, Handler WB, Chronik BA, Santyr GE. A variable field strength system for hyperpolarized noble gas MR imaging of rodent lungs. Concepts Magn Reson B. 2008; 33:124–137.
17. Tsai L, Mair R, Rosen M, Patz S, Walsworth R. An open-access, very-low-field MRI system for posture-dependent ^{3}He human lung imaging. J Magn Reson. 2008; 193:274–285. [PubMed: 18550402]
18. Coffey A, Shchepin R, Truong M, Wilkens K, Pham W, Chekmenev E. An Open-Source Automated Parahydrogen Hyperpolarizer for Molecular Imaging Using ^{13}C Metabolic Contrast Agents. Anal Chem. 2016; 88:8279–8288. [PubMed: 27478927]
19. Hayden M, Bidinosti C, Chapple E. Specific absorption rates and signal-to-noise ratio limitations for MRI in very-low magnetic fields. Concepts Magn Reson. 201(40A):281–294.
20. Bowers C, Weitekamp D. Parahydrogen and Synthesis Allow Drammatically Enhanced Nuclear Alignment. J Am Chem Soc. 1987; 109:5541–5542.
21. Pravica MG, Weitekamp DP. Net NMR alignment by adiabatic transport of parahydrogen addition products to high magnetic field. Chem Phys Lett. 1988; 145:255–258.
22. Natterer J, Bargon J. Parahydrogen Induced Polarization. Prog Nucl Magn Reson Spectrosc. 1997; 31:293–315.
23. Adams R, Aguilar J, Atkinson K, Cowley M, Elliott P, Duckett S, Green G, Khazal I, Lopez-Serrano J, Williamson D. Reversible Interactions with para-Hydrogen Enhance NMR Sensitivity by Polarization Transfer. Science. 2009; 323:1708–1711. [PubMed: 19325111]
24. Hovener J, Schwaderlapp N, Lickert T, Duckett S, Mewis R, Highton L, Kenny S, Green G, Leibfritz D, Korvink J, et al. A Hyperpolarized Equilibrium for Magnetic Resonance. Nat Commun. 2013; 4:2946. [PubMed: 24336292]
25. Barskiy D, Kovtunov K, Koptyug I, He P, Groome K, Best Q, Shi F, Goodson B, Shchepin R, Truong M, et al. *In Situ* and *Ex Situ* Low-Field NMR Spectroscopy and MRI Endowed by SABRE Hyperpolarization. ChemPhysChem. 2014; 15:4100–4107. [PubMed: 25367202]
26. Zhivonitko VV, Skovpin IV, Koptyug IV. Strong ^{31}P nuclear spin hyperpolarization produced via reversible chemical interaction with parahydrogen. Chem Commun. 2015; 51:2506–2509.
27. Truong M, Theis T, Coffey A, Shchepin R, Waddell K, Shi F, Goodson B, Warren W, Chekmenev E. N-15 Hyperpolarization by Reversible Exchange Using SABRE-SHEATH. J Phys Chem C. 2015; 119:8786–8797.
28. Barskiy DA, Shchepin RV, Coffey AM, Theis T, Warren WS, Goodson BM, Chekmenev EY. Over 20% ^{15}N Hyperpolarization in Under One Minute for Metronidazole, an Antibiotic and Hypoxia Probe. J Am Chem Soc. 2016; 138:8080–8083. [PubMed: 27321159]
29. Ardenkjaer-Larsen J, Fridlund B, Gram A, Hansson G, Hansson L, Lerche M, Servin R, Thaning M, Golman K. Increase in Signal-to-noise Ratio of > 10,000 Times in Liquid-state NMR. Proc Natl Acad Sci USA. 2003; 100:10158–10163. [PubMed: 12930897]
30. Ardenkjaer-Larsen J. On the Present and Future of Dissolution-DNP. J Magn Reson. 2016; 264:3–12. [PubMed: 26920825]
31. Barskiy DA, Coffey AM, Nikolaou P, Mikhaylov DM, Goodson BM, Branca RT, Lu GJ, Shapiro MG, Telkki VV, Zhivonitko VV, et al. NMR Hyperpolarization Techniques of Gases. Chem Eur J. 2016; doi: 10.1002/chem.201603884
32. Ardenkjaer-Larsen J, Boebinger G, Comment A, Duckett S, Edison A, Engelke F, Griesinger C, Griffin R, Hilty C, Maeda H, et al. Facing and Overcoming Sensitivity Challenges in Biomolecular NMR Spectroscopy. Angew Chem Int Ed. 2015; 54:9162–9185.
33. Barskiy DA, Salnikov OG, Shchepin RV, Feldman M, Coffey AM, Kovtunov KV, Koptyug IV, Chekmenev EY. NMR SLIC Sensing of Hydrogenation Reactions Using Parahydrogen in Low Magnetic Fields. J Phys Chem C. 2016; doi: 10.1021/acs.jpcc.6b07555
34. Bowers C, Weitekamp D. Transformation of Symmetrization Order to Nuclear Spin Magnetization by Chemical Reaction and Nuclear Magnetic Resonance. Phys Rev Lett. 1986; 57:2645–2648. [PubMed: 10033824]
35. Vinogradov E, Grant AK. Hyperpolarized long-lived states in solution NMR: Three-spin case study in low field. J Magn Reson. 2008; 194:46–57. [PubMed: 18602320]

36. Tayler M, Levitt M. Singlet Nuclear Magnetic Resonance of Nearly-Equivalent Spins. Phys Chem Chem Phys. 2011; 13:5556–60. [PubMed: 21318206]
37. DeVience S, Walsworth R, Rosen M. Preparation of Nuclear Spin Singlet States Using Spin-Lock Induced Crossing. Phys Rev Lett. 2013; 111:173002. [PubMed: 24206484]
38. Theis T, Feng Y, Wu Tl, Warren WS. Composite and Shaped Pulses for Efficient and Robust Pumping of Disconnected Eigenstates in Magnetic Resonance. J Chem Phys. 2014; 140:014201. [PubMed: 24410222]
39. Pravdivtsev AN, Kiryutin AS, Yurkovskaya AV, Vieth HM, Ivanov KL. Robust conversion of singlet spin order in coupled spin-1/2 pairs by adiabatically ramped RF-fields. J Magn Reson. 2016; 273:56–64. [PubMed: 27750072]
40. Kovtunov K, Truong M, Barskiy D, Koptyug I, Coffey A, Waddell K, Chekmenev E. Long-Lived Spin States for Low-field Hyperpolarized Gas MRI. Chem Eur J. 2014; 20:14629–14632. [PubMed: 25263795]
41. Vinogradov E, Grant AK. Long-Lived States in Solution NMR: Selection Rules for Intramolecular Dipolar Relaxation in Low Magnetic Fields. J Magn Reson. 2007; 188:176–182. [PubMed: 17600743]
42. Gutowsky H, Lawrenson I, Shimomura K. Nuclear Magnetic Spin-Lattice Relaxation by Spin-Rotational Interactions. Phys Rev Lett. 1961; 6:349–351.
43. Bloom M, Lipsicas M, Muller B. Proton spin-lattice relaxation in polyatomic gases. Can J Phys. 1961; 39:1093–1109.
44. Grant AK, Vinogradov E. Long-lived states in solution NMR: Theoretical examples in three-and four-spin systems. J Magn Reson. 2008; 193:177–190. [PubMed: 18511314]
45. Stevanato G, Roy SS, Hill-Cousins J, Kuprov I, Brown LJ, Brown RC, Pileio G, Levitt MH. Long-Lived Nuclear Spin States Far from Magnetic Equivalence. Phys Chem Chem Phys. 2015; 17:5913–5922. [PubMed: 25633837]
46. Ahuja P, Sarkar R, Vasos PR, Bodenhausen G. Long-lived States in Multiple-Spin Systems. ChemPhysChem. 2009; 10:2217–2220. [PubMed: 19630056]
47. Pileio G, Concistrè M, Carravetta M, Levitt MH. Long-lived nuclear spin states in the solution NMR of four-spin systems. J Magn Reson. 2006; 182:353–357. [PubMed: 16884939]
48. DeVience S, Walsworth R, Rosen M. Probing Scalar Coupling Differences via Long-Lived Singlet States. J Magn Reson. 2016; 262:42–49. [PubMed: 26717036]
49. Kovtunov K, Barskiy D, Coffey A, Truong M, Salnikov O, Khudorozhkov A, Inozemtseva E, Prosvirin I, Bukhtiyarov V, Waddell K, et al. High-Resolution 3D Proton MRI of Hyperpolarized Gas Enabled by Parahydrogen and Rh/TiO_2 Heterogeneous Catalyst. Chem Eur J. 2014; 20:11636–11639. [PubMed: 24961814]
50. Kovtunov K, Zhivonitko V, Skovpin I, Barskiy D, Koptyug I. Parahydrogen-Induced Polarization in Heterogeneous Catalytic Processes. Top Curr Chem. 2013; 338:123–180. [PubMed: 23097028]
51. Waddell K, Coffey A, Chekmenev E. In Situ Detection of PHIP at 48 mT: Demonstration Using a Centrally Controlled Polarizer. J Am Chem Soc. 2011; 133:97–101. [PubMed: 21141960]
52. Coffey A, Shchepin R, Wilkens K, Waddell K, Chekmenev E. A Large Volume Double Channel H-1-X RF Probe for Hyperpolarized Magnetic Resonance at 0.0475 T. J Magn Reson. 2012; 220:94–101. [PubMed: 22706029]
53. Kovtunov K, Barskiy D, Shchepin R, Coffey A, Waddell K, Koptyug I, Chekmenev E. Demonstration of Heterogeneous Parahydrogen Induced Polarization Using Hyperpolarized Agent Migration from Dissolved Rh(I) Complex to Gas Phase. Anal Chem. 2014; 86:6192–6. [PubMed: 24918975]
54. Kovtunov K, Truong M, Barskiy D, Salnikov O, Bukhtiyarov V, Coffey A, Waddell K, Koptyug I, Chekmenev E. Propane-d(6) Heterogeneously Hyperpolarized by Parahydrogen. J Phys Chem C. 2014; 118:28234–28243.
55. Devience, SJ. Doctoral dissertation. 2014. Nuclear Magnetic Resonance with Spin Singlet States and Nitrogen Vacancy Centers in Diamond.
56. Bond, GC. Metal-catalysed reactions of hydrocarbons. Springer; US, New York: 2005.

57. Salnikov O, Kovtunov K, Barskiy D, Bukhtiyarov V, Kaptein R, Koptyug I. Kinetic Study of Propylene Hydrogenation over Pt/Al_2O_3 by Parahydrogen-Induced Polarization. Appl Magn Reson. 2013; 44:279–288.
58. Barskiy D, Salnikov O, Kovtunov K, Koptyug I. NMR Signal Enhancement for Hyperpolarized Fluids Continuously Generated in Hydrogenation Reactions with Parahydrogen. J Phys Chem A. 2015; 119:996–1006. [PubMed: 25587942]
59. Davis, ME., Davis, RJ. Fundamentals of chemical reaction engineering. Courier Corporation; 2012.
60. Zhou R, Zhao E, Cheng W, Neal L, Zheng H, Quinones R, Hagelin-Weaver H, Bowers C. Parahydrogen-Induced Polarization by Pairwise Replacement Catalysis on Pt and Ir Nanoparticles. J Am Chem Soc. 2015; 137:1938–1946. [PubMed: 25629434]
61. Zhou R, Cheng W, Neal L, Zhao E, Ludden K, Hagelin-Weaver H, Bowers C. Parahydrogen enhanced NMR reveals correlations in selective hydrogenation of triple bonds over supported Pt catalyst. Phys Chem Chem Phys. 2015; 17:26121–26129. [PubMed: 26376759]
62. Zhao E, Zheng H, Ludden K, Xin Y, Hagelin-Weaver H, Bowers C. Strong Metal-Support Interactions Enhance the Pairwise Selectivity of Parahydrogen Addition over Ir/TiO_2. ACS Catal. 2016; 6:974–978.
63. Kuethe DO, Caprihan A, Fukushima E, Waggoner RA. Imaging lungs using inert fluorinated gases. Magn Reson Med. 1998; 39:85–88. [PubMed: 9438441]
64. Kuethe DO, Caprihan A, Gach HM, Lowe IJ, Fukushima E. Imaging obstructed ventilation with NMR using inert fluorinated gases. J Appl Physiol. 2000; 88:2279–2286. [PubMed: 10846046]
65. Goodson B. Nuclear Magnetic Resonance of Laser-polarized Noble Gases in Molecules, Materials, and Organisms. J Magn Reson. 2002; 155:157–216. [PubMed: 12036331]
66. Lilburn DM, Pavlovskaya GE, Meersmann T. Perspectives of hyperpolarized noble gas MRI beyond 3 He. J Magn Reson. 2013; 229:173–186. [PubMed: 23290627]
67. Vuichoud B, Canet E, Milani J, Bornet A, Baudouin D, Veyre L, Gajan D, Emsley L, Lesage A, Copéret C, et al. Hyperpolarization of Frozen Hydrocarbon Gases by Dynamic Nuclear Polarization at 1.2 K. J Phys Chem Lett. 2016; 7:3235–3239. [PubMed: 27483034]
68. Nikolaou P, Coffey A, Walkup L, Gust B, Whiting N, Newton H, Barcus S, Muradyan I, Dabaghyan M, Moroz G, et al. Near-unity nuclear polarization with an open-source Xe-129 hyperpolarizer for NMR and MRI. Proc Natl Acad Sci USA. 2013; 110:14150–14155. [PubMed: 23946420]
69. Nikolaou P, Coffey A, Ranta K, Walkup L, Gust B, Barlow M, Rosen M, Goodson B, Chekmenev E. Multidimensional Mapping of Spin-Exchange Optical Pumping in Clinical-Scale Batch-Mode Xe-129 Hyperpolarizers. J Phys Chem B. 2014; 118:4809–4816. [PubMed: 24731261]
70. Freeman MS, Emami K, Driehuys B. Characterizing and modeling the efficiency limits in large-scale production of hyperpolarized ^{129}Xe. Phys Rev A. 2014; 90:023406. [PubMed: 25400489]
71. Salnikov OG, Barskiy DA, Coffey AM, Kovtunov KV, Koptyug IV, Chekmenev EY. Efficient Batch-Mode Parahydrogen-Induced Polarization of Propane. ChemPhysChem. 2016; 17:3395–3398. [PubMed: 27459542]

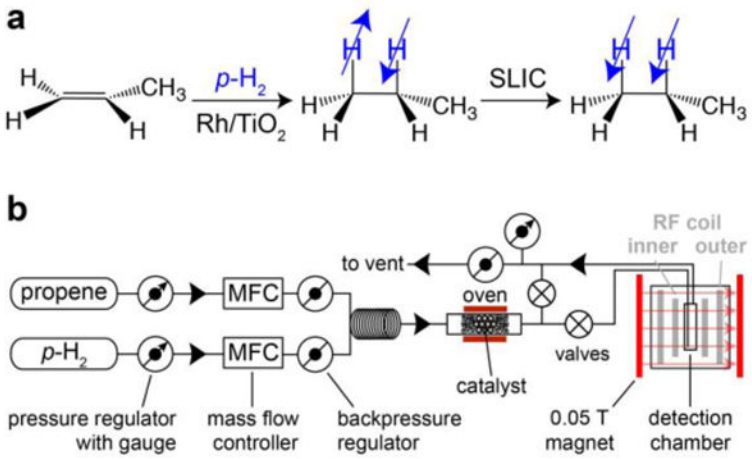

Figure 1.

a) Molecular diagram of parahydrogen (p-H_2) addition to propylene over Rh/TiO_2 at 0.05 T resulting in the formation of pseudo-singlet long-lived spin states (LLSS) of propane, followed by the application of the spin-lock induced crossing (SLIC) sequence to transform LLSS into observable magnetization and to detect the NMR signal. b) Schematic diagram of the experimental setup employed to perform p-H_2 addition to propylene and to detect LLSS of propane produced at 0.05 T using the SLIC sequence. Note that separate $^1H/^1H$ Rx and Tx coils were used, with the internal solenoid (Rx) geometrically decoupled from the outer saddle-shaped coil (Tx) by orienting them orthogonally (in addition to mutual orthogonality of B_1 fields of each RF coil to the main B_0 field, see SI).

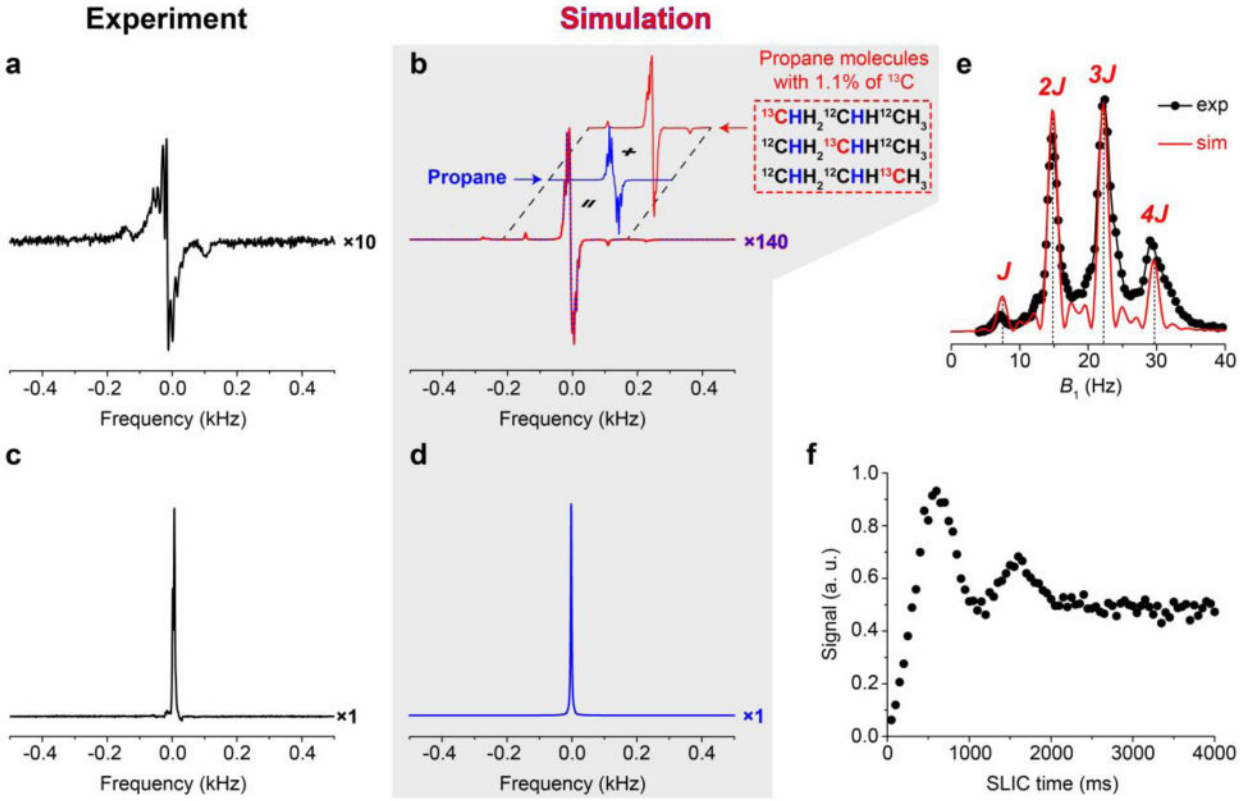

Figure 2.

a) ^{1}H NMR spectrum of HP propane recorded at 0.05 T after application of a $\pi/2$ hard RF pulse; HP propane is obtained from propylene via pairwise *p*-H_2 addition over Rh/TiO_2 catalyst. b) Simulation of ^{1}H NMR spectrum of HP propane (after application of a $\pi/2$ hard RF pulse): blue trace – HP propane population without a ^{13}C nucleus; red trace – HP propane containing 1.1% (natural ^{13}C abundance) of randomly distributed ^{13}C nuclei; blue-red trace is the sum of blue and red traces shown behind it. c) ^{1}H NMR spectrum of HP propane recorded at 0.05 T after application of SLIC RF pulse with B_1 of 22.2 Hz (SNR ~ 730); HP propane is obtained from propylene via pairwise *p*-H_2 addition over Rh/TiO_2 catalyst. d) Simulation of ^{1}H NMR spectrum of HP propane using a SLIC RF pulse with B_1 of ~22.2 Hz. Note the vertical scaling factor of 10 for spectrum (a) compared to spectrum (c), and the factor of 140 scaling for spectrum (b) compared to spectrum (d). e) Experimentally measured (black circles and trace) and theoretically calculated (red trace) dependence of the SLIC induced HP propane signal on B_1 amplitude at the SLIC RF pulse duration (τ_{slic}) of 0.5 s at 0.05 T. f) Experimentally measured dependence of the SLIC induced HP propane signal on the SLIC RF pulse duration at B_1 amplitude of 22.2 Hz.

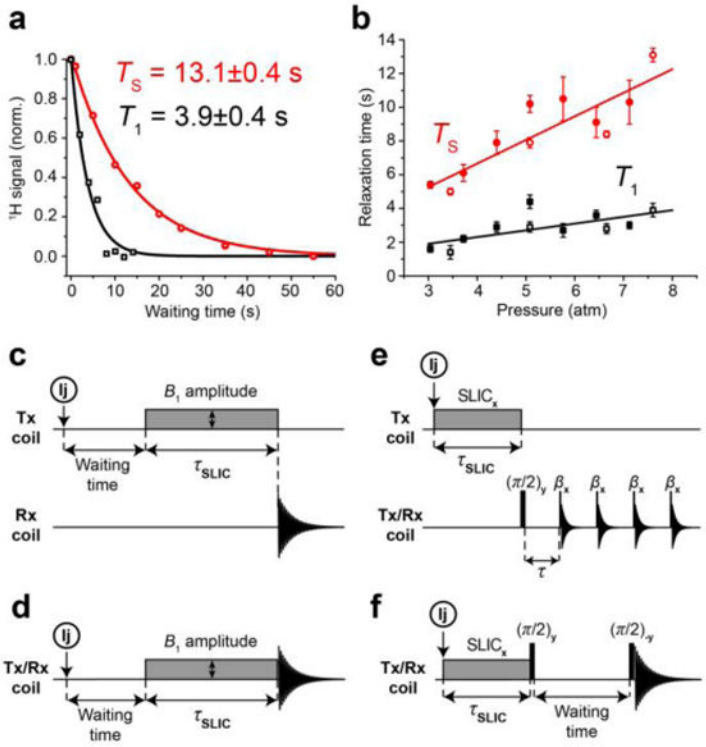

Figure 3.

a) Examples of T_1 (black symbols and trace) and T_S (red symbols and trace) measurements of gaseous HP propane at ~7.6 atm. b) Measured T_1 (black symbols and trace) and T_S (red symbols and trace) of gaseous propane at various pressures. Empty circles and squares show the results obtained using the setup described in Figure 1b (second experimental arrangement, see Section 2.2), filled circles and squares show results obtained using the first experimental arrangement (see Section 2.2). c) Sequence of events for propane T_S measurements using the two channel ^{1}H/^{1}H probe (experimental data points are represented by empty red circles in Figure 3b): Injection (Ij) of the propane into the detection chamber, flow cessation in the detection chamber and a waiting time period of variable duration, low-amplitude RF field irradiation (SLIC) for the time τ_{slic} on the transmit (Tx) coil followed by signal acquisition using the Tx/Rx coil. d) Sequence of events for propane T_S measurement using a single-channel ^{1}H probe (experimental data points are represented by filled red circles in Figure 3b). e) Sequence of events for propane T_1 measurements using a two channel ^{1}H/^{1}H probe (experimental data points are represented by empty black squares in Figure 3b): Injection (Ij) of HP propane into the detection chamber, flow cessation and immediate application of low-power irradiation (SLIC) for duration τ_{slic} on the transmit (Tx) coil followed by a $\pi/2$ pulse and a train of small-angle excitation pulses (β=10°) with time delay τ. f) Sequence of events for propane T_1 measurement using a single-channel ^{1}H probe (experimental data points are represented by filled black squares in Figure 3b).